Available online at www.sciencedirect.com
SCIENCE DIRECT®
Catalysis Today 114 (2006) 112–124
CATALYSIS TODAY
www.elsevier.com/locate/cattod

# $NO_x$ adsorption on $Pt/K/Al_2O_3$

Todd J. Toops *, D. Barton Smith, William P. Partridge

*Oak Ridge National Laboratory, Fuels, Engines and Emissions Research Center, 2360 Cherahala Blvd., Knoxville, TN 37932-1563, United States*

Available online 10 March 2006

**Abstract**

This study explores $NO_x$ storage in a $Pt/K/Al_2O_3$ lean $NO_x$ trap (LNT) catalyst using in situ diffuse reflectance Fourier transform infrared spectroscopy (DRIFTS) in conjunction with chemisorption. The combination of these techniques allows the quantification of surface species for this catalyst system. A free nitrate ion, $NO_3^-$, is the primary form of stored $NO_x$ on the potassium phase at all temperatures, but there was significant nitrite formation observed below 200 °C during short adsorption times. The $NO_2$ saturation storage on $Pt/K/Al_2O_3$ decreases from 6.7 μmol/m$^2$ at 150 °C to 1.8 μmol/m$^2$ at 400 °C, and DRIFTS indicates that the equilibrated surface species are identical over this entire temperature range. While the final state of $Pt/K/Al_2O_3$ is identical at all temperatures, the rates and observed surface species change significantly. After 1 min uptake, $NO_x$ adsorption varies from 0.35 μmol/m$^2$ at 150 °C to a maximum of 3.2 μmol/m$^2$ at 250 °C, and at 400 °C the adsorption decreases to 1.1 μmol/m$^2$. This temperature sweep illustrates the limiting regimes associated with $NO_x$ adsorption: kinetic limitations at lower temperatures due to the strength of the Pt–O bond and insufficient storage sites at higher temperatures. This study propose three routes for the storage of $NO_x$ on $Pt/K/Al_2O_3$, two of them involving a potassium storage site adjacent to Pt sites, and a third route that involves a form of $NO_2$ disproportionation on storage sites irrespective of their proximity to Pt.


*Keywords:* Lean $NO_x$ traps; DRIFTS; Chemisorption; Potassium; $NO_x$ storage

## 1. Introduction

Lean $NO_x$ Trap (LNT) catalyst systems are a leading solution for the impending stricter diesel emissions regulations [1]. They are based on the ability of alkali and alkaline earth elements to trap $NO_x$ under lean conditions in the form of nitrates [2–4]. The stored nitrates are then released and reduced in a brief rich interval to obtain benign $N_2$. These catalysts require an oxidation component, typically a noble metal like Pt, a storage component, commonly Ba, and a high surface area support such as $\gamma$-$Al_2O_3$. Potassium, especially in conjunction with Ba, is another element that has shown potential as a storage component with a significant benefit at higher temperatures where the K-based nitrate is more stable than the typical Ba nitrate [5–9]. LNTs containing Ba have a typical operating regime of 200–450 °C [10], and the addition of an alkali washcoat component has been shown to increase operation up to 575 °C [8,9].

Numerous studies have shown that K has a strong interaction with $Al_2O_3$ supports [11–14], and recent studies have begun to elucidate the contributions of the individual components to $NO_x$ storage on K-based LNTs [15–17]. This study focused on expanding this understanding of $NO_x$ adsorption on a catalyst consisting of Pt and K phases on an $Al_2O_3$ support across the typical emission temperatures of heavy-duty diesel engines, 150–400 °C. Studies of Ba-based LNTs have shown that slow oxidation of NO to $NO_2$ on Pt and the subsequent immobility of O and $NO_2$ limit storage below 200 °C; at temperatures above 450 °C the limiting factor seems to be inadequate strong $NO_x$ adsorption sites [18–21]. Additional Ba-based studies have proposed several mechanistic adsorption routes in the transition from gas-phase $NO_x$ to stored nitrates, which generally fall into three categories [19,21–29]:

- Nitrite formation near Pt followed by oxidation to nitrate.
- Direct nitrate formation on the Ba-phase from $NO_2$ and an adsorbed O atom near a Pt site.
- Disproportionation of Ba-nitrite species to form nitrates and desorb an NO molecule irrespective of Pt proximity.

It has been surmised that the routes involving intermediate nitrites have a diminishing role above 300 °C due to the thermal

* Corresponding author. Tel.: +1 865 946 1207; fax: +1 865 946 1354.
*E-mail address:* toopstj@ornl.gov (T.J. Toops).

0920-5861/$ – see front matter 
doi:10.1016/j.cattod.2006.02.006

instability of the nitrite. It has also been proposed that the adsorption route on sites that are not adjacent to Pt have an increased role in the later stages of adsorption. These limiting ranges and key mechanistic steps have not previously been reported on K-based catalysts, and it is the goal of this study to elucidate these reactions. Diffuse reflectance infrared Fourier transform spectroscopy (DRIFTS) is the primary analytical tool used in this study, and chemisorption was used to quantify certain features of the DRIFT spectra related to $NO_x$ and $CO_2$ adsorption using an approach detailed elsewhere [15].

## 2. Experimental

The model catalysts used in this experiment were $\gamma$-$Al_2O_3$, 1% Pt on $\gamma$-$Al_2O_3$ (Pt/$Al_2O_3$), 8.0% $K_2CO_3$ on $\gamma$-$Al_2O_3$ (K/$Al_2O_3$), and the complete $NO_x$ adsorber catalyst, 8% $K_2CO_3$ on 1% Pt/$Al_2O_3$ (Pt/K/$Al_2O_3$).[1] An 8% loading of $K_2CO_3$ corresponds to 64% of a monolayer. For comparison, a catalyst formulation of 5.3% $Ba(NO_3)_2$ on 1% Pt/$Al_2O_3$ (Pt/Ba/$Al_2O_3$) was also tested. All percentages listed above are mass-based. The catalyst formulations are summarized in Table 1 along with results from $H_2$ chemisorption and $N_2$ physisorption measurements. Before experimentation all catalysts underwent a pretreatment with 50 $cm^3$ (STP)/min (sccm) of 1% $H_2$ in $N_2$ (99.999% pure) at 450 °C; the length of this pretreatment depended on the catalyst formulation. The pretreatment established a consistent starting point for each experiment.

The DRIFTS system has been detailed in earlier papers [15,30]. It consists of a *MIDAC* model M2500 FT-IR spectrometer coupled to a *Harrick Scientific* barrel ellipsoidal mirror DRIFT accessory with an integrated stainless-steel reaction cell. The catalyst samples were reacted under carefully controlled temperature and gas-flow conditions. The system can be heated to 525 °C, is configured to allow up to 10% $H_2O$ in the feed, and is typically operated at slightly below atmospheric pressure, ca. 500 Torr, to prevent stagnation in the cell and to sustain the seal between the removable hemispherical ZnSe dome and the cell body. *Tylan General* mass flow controllers establish the inlet gas concentrations, in conjunction with a sparger system submerged in a *NESLAB* RTE-110 recirculating constant temperature bath that controls the inlet concentration of $H_2O$. A *General Eastern* DewPro humidity sensor is used to verify the water concentration. The reactant gases used in the measurements had the following purities: $CO_2$ (99.999%), 1% $H_2$ in $N_2$ (99.999%), 1000 ppm NO in $N_2$ (99.0%), 1000 ppm $NO_2$ in $N_2$ (99.0%), and $N_2$ (99.999%).

Before exposure to the $NO_x$ gas mixtures, each catalyst sample was pretreated in the cell by heating to 450 °C and reacting with a 50 sccm flow of 1% $H_2/N_2$. The pretreatment continued until the carbonate absorbance features in the FT-IR spectra were diminished and stabilized at their minimum intensities. The pretreatment was typically accomplished in one hour; pretreatment for longer periods produced no measurable reduction in carbonate peak intensities. Following pretreatment, the 1% $H_2/N_2$ flow was continued while the sample was cooled to the adsorption temperature of interest, between 150 and 400 °C. At the adsorption temperature, the cell was sealed with stagnant 1% $H_2/N_2$ pretreatment gas mixture, and the reactant gas mixture was routed through the bypass loop for a period of 5 min to stabilize the gas mixture concentrations. A background DRIFT spectrum was acquired just before introducing the reactant mixture. This file was used to convert the reflectance files into absorbance units using:

$$\text{absorbance} = -\log_{10}\left[\frac{\text{sample file}}{\text{background file}}\right] \quad (1)$$

At each temperature, the catalyst was allowed to saturate in 300 ppm $NO_2$ flowing at 50 sccm until equilibrium, usually overnight. The spectra obtained at saturation were correlated with $NO_2$ chemisorption values from the corresponding temperature and pressure to determine the coefficients of adsorption for the catalyst at each temperature. The catalyst was then preheated again to reestablish the initial reduced condition. After cooling back to the adsorption temperature of interest, lean $NO_x$ adsorption was initiated with 300 ppm NO, 12% $O_2$, 5% $CO_2$, and 5% $H_2O$ at 50 sccm. This sequence establishes a maximum $NO_x$ adsorption value with the first step which is used to calibrate the data recorded with the simulated exhaust in the second experiment.

The chemisorption and physisorption analyzer used for surface area determinations, measuring active metal dispersions, and quantifying adsorbates is a conventional volumetric system that was developed in-house. The analyzer, described in full detail elsewhere [15], consists of a pyrex manifold for introducing $H_2$, $CO_2$ and $N_2$ gases, a U-shaped quartz sample cell, and an oil-less high-vacuum system that provides base pressures in the low $10^{-7}$ Torr range when evacuating the manifold and removing adsorbates from samples. The system was configured to allow gas flow through the sample cell using an MKS Type 247 control unit with MKS mass flow controllers. All o-rings in the Pyrex/stainless steel system were constructed of perfluoroelastomers to withstand $NO_2$. The sample cell was heated with a vertical furnace in conjunction with a PID temperature controller. Isotherm pressure readings were obtained using a Mensor 6100 DPT pressure transducer with 0.01% full-scale accuracy. Fresh samples were dried for 1 h at 150 °C in 50 sccm He to remove adsorbed $H_2O$; the samples were then weighed and reloaded in the sample cell. The dried catalysts were pretreated in 50 sccm of 1% $H_2/N_2$ at 450 °C overnight, evacuated to the base pressure, and then cooled to the appropriate temperature under vacuum. Once thermal stability was achieved in the sample cell, the probe gas was introduced. The pure gas was then allowed to equilibrate with the surface at pressures between 50 and 250 Torr. This was repeated to record several data points and a linear relationship between molar uptake and pressure was achieved. Where applicable, the reversible uptake was measured by evacuating to the base pressure for 1 h and repeating the procedure.

[1] *EmeraChem* provided all catalysts for this study.

Table 1
Formulation and characterization of studied catalysts

| Catalyst | Pt (wt.%) | $K_2CO_3$ (wt.%) | $Ba(NO_3)_2$ (wt.%) | $Al_2O_3$ (wt.%) | Dispersion ($Pt_s/Pt_T$) | Surface area ($m^2/g$) |
|---|---|---|---|---|---|---|
| $\gamma$-$Al_2O_3$ | – | – | – | 100 | – | 160 |
| $Pt/Al_2O_3$ | 1.0 | – | – | 99 | 37% | 151 |
| $K/Al_2O_3$ | – | 8.0 | – | 92 | – | 146 |
| $Pt/K/Al_2O_3$ | 1.0 | 8.0 | – | 91 | 18% | 149 |
| $Pt/Ba/Al_2O_3$ | 1.0 | – | 5.3 | 94 | 23% | 150 |

$H_2$ chemisorption was used to calculate the Pt dispersion, i.e. percentage of Pt surface atoms ($Pt_S$) compared to total Pt atoms in the sample ($Pt_T$), based on the irreversibly adsorbed hydrogen uptake and an H:$Pt_S$ ratio of 1. The chemisorption apparatus was also used to determine a quantitative standard for calibration of the DRIFT-measured concentration of catalyst surface species in terms of $\mu mol/m^2$. The calibration value for carbon-based adsorbates was obtained with $CO_2$ chemisorption and the value for the nitrate features was obtained with $NO_2$ chemisorption, both at 250 °C. Accurate chemisorption measurements of $NO_2$ required an additional consideration due to the dimerization of $NO_2$ to form $N_2O_4$ in the gas phase. This was carefully considered during the NO uptake measurements and the details that were included in this measurement are discussed elsewhere [15].

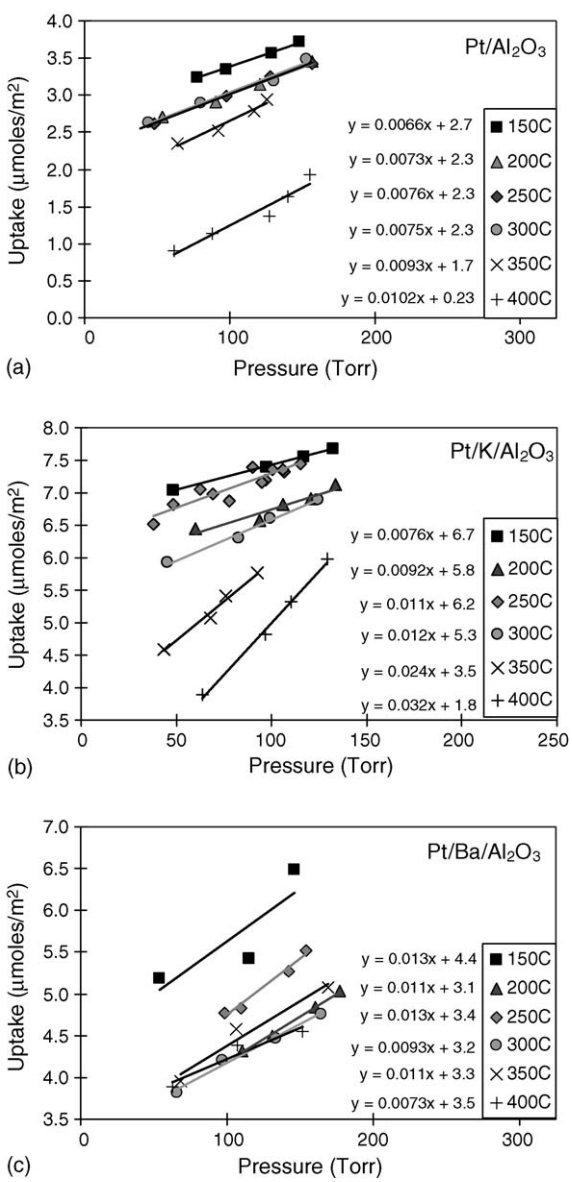


Fig. 1. $NO_2$ isotherms taken between 150 and 400 °C for: (a) $Pt/Al_2O_3$, (b) $Pt/K/Al_2O_3$, and (c) $Pt/Ba/Al_2O_3$.

## 3. Results

The basis for quantifying the DRIFT spectra is $NO_2$ chemisorption at saturation, which is measured in a static chemisorption cell using $NO_2$ for $Pt/K/Al_2O_3$, $Pt/Al_2O_3$ and $Pt/Ba/Al_2O_3$ catalysts. The isotherms are shown in Fig. 1 between 150 and 400 °C, and the corresponding maximum capacity of the catalysts based on the extrapolated isotherms at 0.23 Torr (i.e. 300 ppm at 760 Torr) is shown in Fig. 2. Since the K and Ba loadings vary significantly, the results are also displayed on a normalized molar basis for these two catalysts on the right axis in Fig. 2. This comparison on the right axis also includes adsorption of $NO_2$ on the alumina-phase, and illustrates adsorptions greater than stoichiometry for both K (1:1) and Ba (2:1) at 25 °C where the static $NO_2$ adsorption is greatest on alumina.

The focus of this paper is on $Pt/K/Al_2O_3$, so the detailed DRIFTS analysis was only performed on this LNT. The DRIFT spectra following adsorption of 50 sccm of 300 ppm $NO_2$ in $N_2$ overnight, are shown for each temperature between 150 and 400 °C in Fig. 3, and the corresponding spectral assignments are given in Table 2 [17,23,31–40]. Each spectra is recorded in

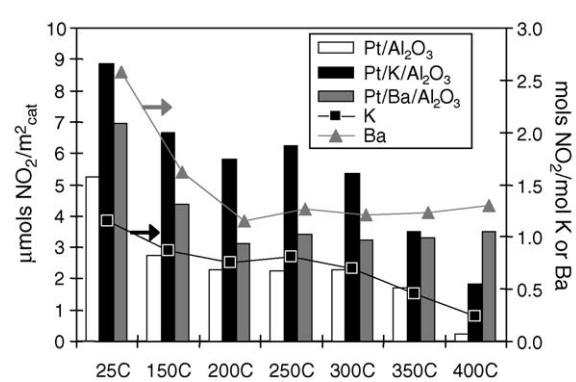


Fig. 2. $NO_2$ uptake at 0.23 Torr for: (▭) $Pt/Al_2O_3$, (▬) $Pt/K/Al_2O_3$, and (▬) $Pt/Ba/Al_2O_3$. The right axis is the molar uptake normalized to molar (■) K and (▲) Ba loading.

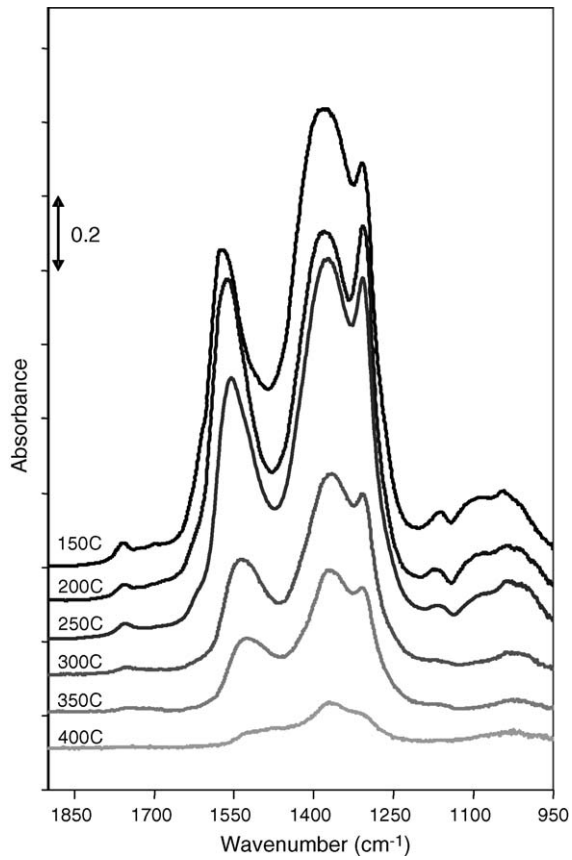


Fig. 3. DRIFT spectra of $Pt/K/Al_2O_3$ after saturating with 300 ppm $NO_2$ at 150, 200, 250, 300, 350, and 400 °C. Experimental conditions: 50 sccm of 300 ppm $NO_2$ in $N_2$; spectra recorded after 15 h of adsorption and referenced to $t = 0$.

situ at the temperature of interest. The alumina-based structure is well detailed in the literature and apparent in the spectra reported elsewhere [23,31–37]; however, when adsorber material is present, i.e. K or Ba, the structure is minimal compared to the adsorber-based nitrate. This loss of detail makes identification of the alumina phase nitrates impossible, and thus was not specifically identified. The simplicity of the DRIFT spectra on $Pt/K/Al_2O_3$ (at saturation the ionic nitrate at 1380 $cm^{-1}$ is the only significant $NO_x$ adsorbate on the K-phase) allows the quantification of the spectral feature using the chemisorption value at 0.23 Torr at each temperature. Although the spectral features are significantly diminished at the higher temperatures, with respect to absorbance units, the feature locations are identical at saturation for each temperature. The values in Fig. 2 are for the overall uptake (including storage on alumina), but the values used for the quantification of the area associated with 1380 $cm^{-1}$ is only the K-based adsorption. This is based on the alkali phase covering 65% of the surface and the remaining alumina-phase chemisorbing similarly to pure alumina, and also described in detail elsewhere [15]. Since the DRIFT spectra are temperature dependent, absorption coefficients were determined at each temperature and are listed in Table 3. The units are based on the normalized concentration of $NO_2$ adsorbed (μmol $NO_2/m^2$) divided by the area under the $NO_3^-$ spectral feature (absorbance $cm^{-1}$).

Table 2
Assignments of the IR absorption bands for adsorbed species on the $Pt/K/Al_2O_3$ catalyst

| Peak position ($cm^{-1}$) | Infrared vibration | Structure |
|---|---|---|
| Nitrogen-based adsorbates [17,23,31–37,40] | | |
| Alumina-based nitrates | | |
| 1525 | Overlapping | n/a |
| 1320 | Overlapping | n/a |
| Free nitrite ion | | |
| 1250 | Asymmetric stretch | $NO_2^-$ |
| Free nitrate ion | | |
| 1380 | Asymmetric stretch ($\nu_3$) | $NO_3^-$ |
| 1750 | Combination band ($\nu_1 + \nu_4$) | |
| Carbon-based adsorbates [31,38,39] | | |
| Carboxylate ion, $CO_2^-$ | | |
| 1599 | $CO_2$ asymmetric stretch | 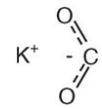 |
| 1310 | $CO_2$ symmetric stretch | |
| Chelating bidentate carbonate | | |
| 1545 | C=O stretch | 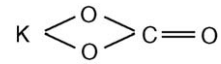 |
| 1363 | $CO_2$ asymmetric stretch | |

Similar chemisorption and DRIFTS saturation experiments were performed with $CO_2$. The chemisorption isotherms are displayed in Fig. 4 for the $Pt/Al_2O_3$ and the K- and Ba-based LNTs, and the uptakes at 38 Torr $CO_2$ (i.e. 5% at 760 Torr) shown in Fig. 5, with the normalized uptake for the LNTs on the right axis. The catalysts show decreasing uptake with increasing temperature except for a marked increase for $Pt/Ba/Al_2O_3$ at 400 °C.

In this study, the various saturation spectra are primarily used to quantify the spectral features associated with nitrate formation and to identify the competing nature of $CO_2$. However, the most important time frame for LNTs is the first couple of minutes of adsorption, so the initial spectra have the most significance. Fig. 6 shows these early stages of adsorption while flowing 50 sccm of 300 pppm NO, 12% $O_2$, 5% $CO_2$ and 5% $H_2O$; the gas phase $H_2O$ spectral features have been subtracted from these features. Fig. 6(a) and (b) shows the slow adsorption at 150 °C, and the prevalence of significant quantities of nitrites throughout the first hour of adsorption. It is also evident between 10 and 60 min the nitrite, 1250 $cm^{-1}$, begins to decrease; in fact, the area associated the nitrite

Table 3
Infrared absorption coefficients for the ionic nitrate asymmetric stretch (1380 $cm^{-1}$) between 150 and 400 °C

| Temperature (°C) | $K–NO_3^-$ absorption coefficient (μmol $NO_2/m^2$)(cm/Absorbance) |
|---|---|
| 150 | 0.028 |
| 200 | 0.031 |
| 250 | 0.031 |
| 300 | 0.051 |
| 350 | 0.051 |
| 400 | 0.093 |

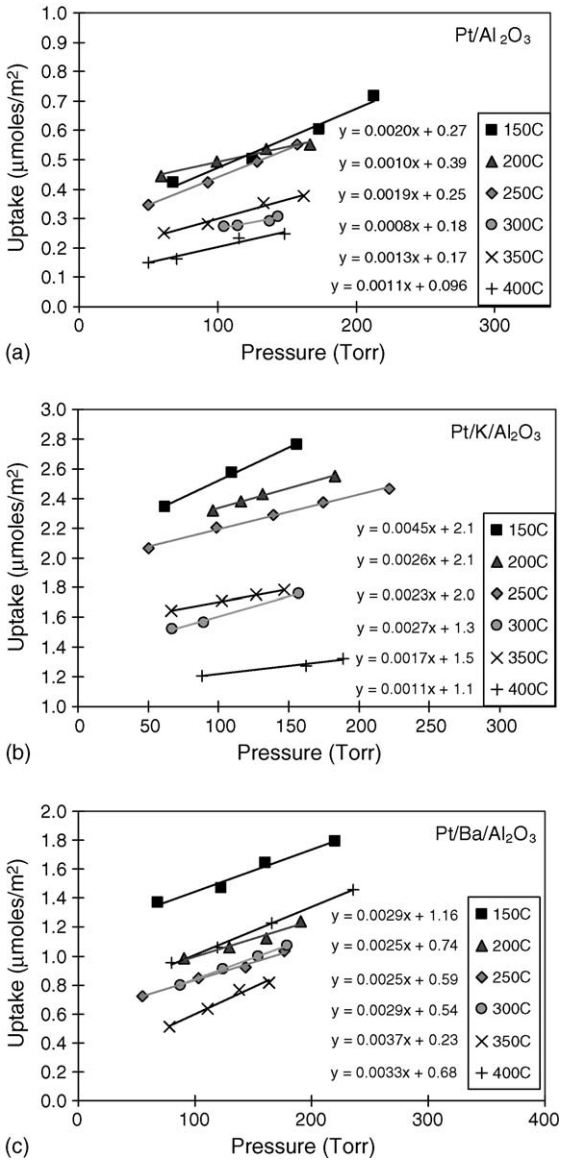


Fig. 4. $CO_2$ isotherms taken between 150 and 400 °C for: (a) $Pt/Al_2O_3$, (b) $Pt/K/Al_2O_3$, and (c) $Pt/Ba/Al_2O_3$.

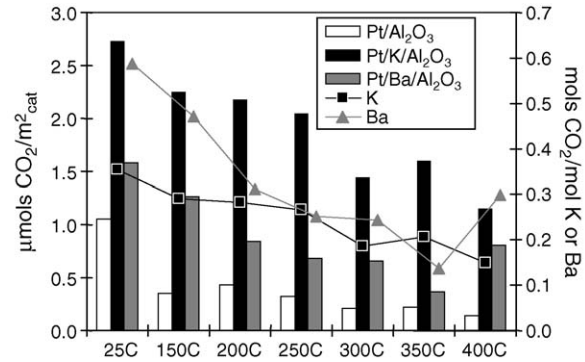


Fig. 5. $CO_2$ uptake at 38 Torr for: (▭) $Pt/Al_2O_3$, (▬) $Pt/K/Al_2O_3$, and (▬) $Pt/Ba/Al_2O_3$. The right axis is the molar uptake normalized to molar (■) K and (▲) Ba loading.

decreases by 22%. This decrease is not immediately evident in Fig. 6(a) if only looking at peak height, but the contribution of the nitrate peak at 1380 $cm^{-1}$ to the height is more significant at 60 min than it is after 10 min, i.e. there is a contribution to the peak height at 1250 $cm^{-1}$ from the lorentzian 1380 $cm^{-1}$ peak. Based on this observation it is evident that the peak area associated with the nitrite at 1250 $cm^{-1}$ is diminished. Above 200 °C, the nitrite is not a significant feature in the spectra, even at early adsorption times. $CO_2$ adsorption is much more prevalent at 150 °C and at $T \geq 200$ °C, $NO_x$ adsorption clearly begins to dominate over $CO_2$; above 300 °C there is a negligible amount of $CO_2^-$ formation.

The results presented in Fig. 6 are summarized and quantified in Figs. 7 and 8. Fig. 7 quantifies the amount of $NO_x$ adsorbed on K with respect to time and temperature, and a volcano-like structure is apparent with a common maximum at 250 °C. Fig. 8 shows the uptake of $NO_x$ from the simulated exhaust conditions relative to the saturation values without $CO_2$ competition from Fig. 2. It is apparent that above 250 °C the catalyst uses ~40% of the net adsorption sites available in just over a minute of adsorption. The maximum in this figure occurs at a lower temperature than the maximum $NO_x$ conversion reported elsewhere [8,9]; however, this is not surprising since the results presented here do not account for the regeneration of the catalyst, i.e. the rich portion of the LNT cycle. The $NO_x$ conversion maximum for the entire cycle incorporates the kinetics of adsorption and $NO_x$ reduction, which results in a higher temperature of maximum operation.

To investigate the rates of nitrate formation without the NO oxidation step, the adsorption of $NO_2$ in the presence and absence of $O_2$ was monitored over $Pt/K/Al_2O_3$ at 250 °C. The DRIFT spectra displayed in Fig. 9 shows that although the NO–$NO_2$ partitioning of the feed $NO_x$ does not change the final adsorbed nitrate form, the rate of adsorption is significantly affected by feed $NO_x$ partitioning; this is further demonstrated in Fig. 10. One of the interesting points in these figures is the comparison of NO-only to NO + $O_2$, where the rate of uptake is considerably slower in the absence of $O_2$. This observation is not surprising since it is widely accepted that NO must be oxidized to $NO_2$ for effective adsorption, but it is surprising that NO is apparently being oxidized and stored with surface-born oxygen. Clearly this LNT is effectively oxidizing the NO to $NO_2$ in the presence of $O_2$ since the NO + $O_2$ rate of adsorption is as fast as the $NO_2$ + $O_2$ rate. Another interesting point in this series of experiments is the comparison of $NO_2$ + $O_2$ to $NO_2$-only, where the importance of excess $O_2$ on the nitrate formation at adsorption times less than 60 min is illustrated. This effect will be discussed fully in the next section.

A final series of experiments was performed to elucidate the key steps in the adsorption of NO and $NO_2$ in the presence and absence of $O_2$ over a Pt-free adsorber, $K/Al_2O_3$. Fig. 11 shows the DRIFTS spectra for this series of experiments, which were a bit more complicated than the previous results. The adsorption of NO in the absence of $O_2$ yielded no measurable nitrates after flowing for several hours, and therefore was not displayed. This observation illustrates that Pt plays a role in liberating surface

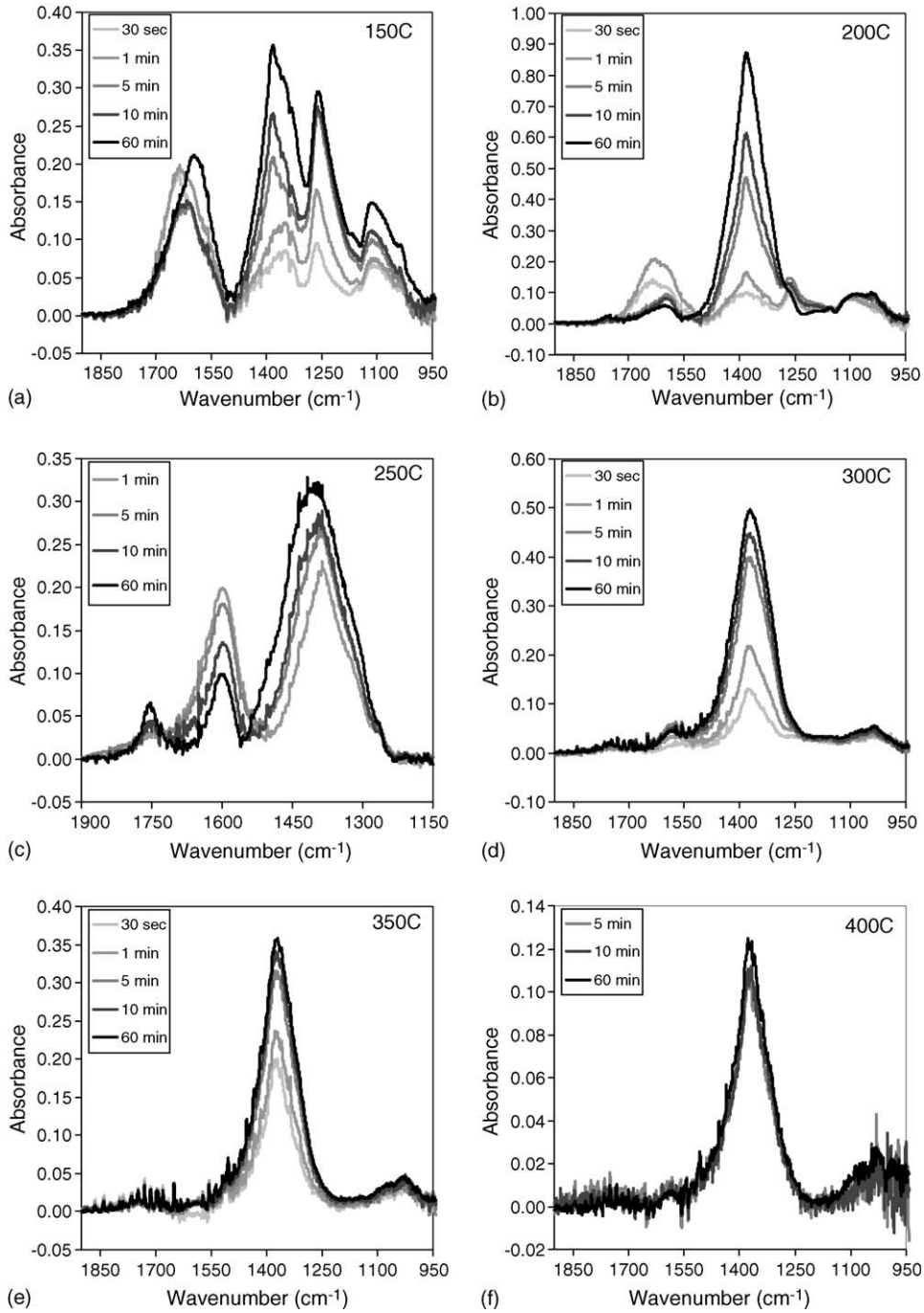


Fig. 6. DRIFT spectra of $Pt/K/Al_2O_3$ during $NO_x$ storage at: (a) 150 °C, (b) 200 °C, (c) 250 °C, (d) 300 °C, (e) 350 °C, and (f) 400 °C. Experimental conditions: 50 sccm of 300 ppm NO 12% $O_2$, 5% $CO_2$, 5% $H_2O$ in $N_2$; spectra recorded after times referenced on graphs with spectra at $t = 0$ subtracted; gas-phase $H_2O$ is also subtracted from spectra.

oxygen for the formation of nitrates from NO in the absence of $O_2$ over $Pt/K/Al_2O_3$, Fig. 9(a). Fig. 11(a) illustrates that in the presence of $O_2$, NO oxidation and subsequent storage is very slow, and that this adsorption path does not play a significant role in the formation of nitrates at sites not proximal to Pt. In the presence of $NO_2$, the spectra are more complicated as negative absorption is apparent at wavenumbers below 1300 $cm^{-1}$ after 60 min of adsorption. This makes quantification difficult and unreliable, so to compare different relative rates of adsorption the height with respect to maximum nitrate formation is plotted in Fig. 12. Figs. 11 and 12 illustrate that nitrates are able to form away from Pt, but require formation of $NO_2$; and as with sites proximal to Pt, $O_2$ promotes nitrate formation at sites away from Pt. None of these tests showed significant nitrite formation, so to investigate this 300 ppm $NO_2$ was adsorbed on $K/Al_2O_3$ at 150 °C at 50 sccm. The DRIFT spectra in Fig. 13 demonstrate that nitrites are prevalent in the early stages of adsorption, as was the case with $Pt/K/Al_2O_3$.

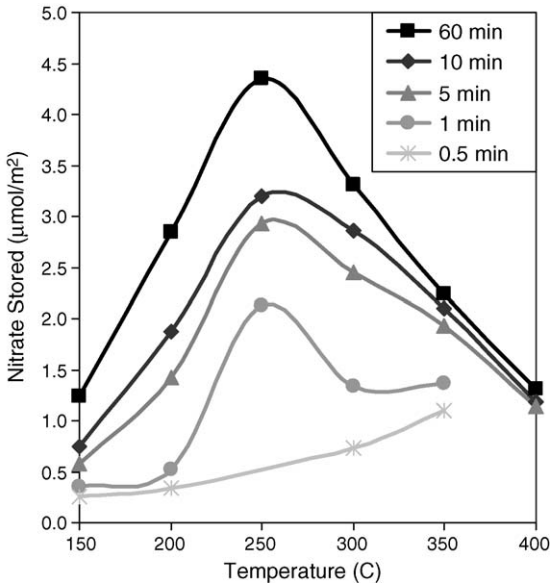


Fig. 7. Nitrate formation on the K-phase of $Pt/K/Al_2O_3$ between 150 and 400 °C after 0.5, 1, 5, 10, and 60 min. Values are based on the quantification of the DRIFT spectra in Fig. 6.

## 4. Discussion

Even the simple model LNTs discussed here show that these multi-component catalysts have very complex behavior. As such, the route to adsorption cannot be described through a simple mechanism involving gas species and a single catalytic site, or even a single route for that matter. There are several distinctly different catalytic sites on each LNT formulation, and each one has a role in the storage of $NO_x$. Several groups have studied the $Pt/Ba/Al_2O_3$ catalyst system at length and have proposed that the three key routes to $NO_x$ storage are barium nitrite formation near Pt which is then oxidized to a nitrate, direct barium nitrate formation near a Pt site, and the disproportionation of Ba-nitrite species leading to nitrates and desorbed NO molecule [19,21–29]. How these routes correspond to $Pt/K/Al_2O_3$ will be discussed below with respect to the three categories of sites, i.e. surface platinum, potassium sites adjacent to Pt, and potassium sites away from Pt. Since the alumina component plays a minor role in the storage of $NO_x$ in the presence of $H_2O$ [15], it will be omitted from consideration. The discussion is divided into the three key steps of $NO_x$ storage: NO oxidation to $NO_2$, nitrite formation, and nitrate formation. An additional section is included to elucidate the activation of the K-phase by oxygen.

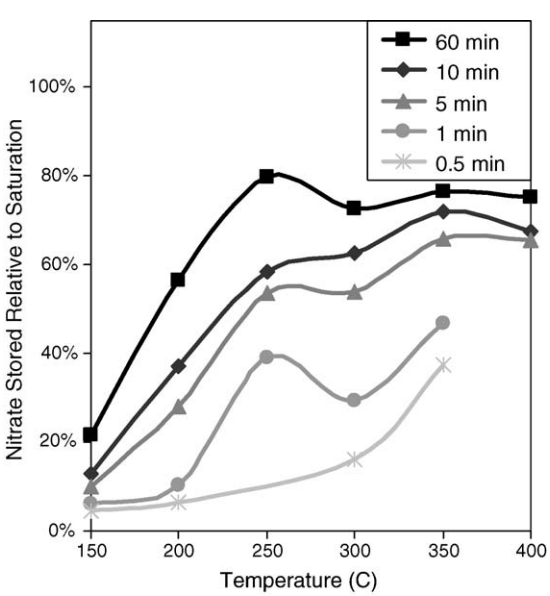


Fig. 8. Nitrate adsorption normalized to the saturation uptake on the K-phase of $Pt/K/Al_2O_3$ between 150 and 400 °C after 0.5, 1, 5, 10, and 60 min.

### 4.1. NO oxidation

The importance of oxidizing NO to $NO_2$ is evident in the $K/Al_2O_3$ experiments in Fig. 11, where only $NO_2$ is effectively adsorbed. These experiments also illustrate the inability of NO to be oxidized to $NO_2$ without Pt. The oxidation of NO to $NO_2$ over Pt has been widely studied, especially with respect to $Pt/Al_2O_3$ systems. A couple of recent studies have focused on the oxidation below 200 °C, where the kinetics are rate-limited by desorption of oxygen from Pt [41,42]. The following mechanism has been proposed:

$$NO_{(g)} + Pt \rightleftharpoons Pt\text{-}NO \quad (2)$$

$$O_{2(g)} + Pt \rightarrow Pt{-}O_2 \quad (3)$$

$$Pt{-}O_2 + Pt \rightarrow 2Pt{-}O \quad (4)$$

$$Pt\text{-}NO + Pt\text{-}O \rightleftharpoons 2\,Pt + NO_{2(g)} \quad (5)$$

Mulla et al. have a convincing argument that the most abundant surface intermediate (MASI) is Pt–O, and that the equilibrium in Eq. (5) heavily favors the left side at lower temperatures [42]. Above 200 °C, Pt–O can still be viewed as the MASI on the Pt sites, but at the higher temperatures it has increased surface mobility leading to higher reactivity. The benefits of this increased mobility also impact the formation of nitrites and nitrates independent of $NO_2$ formation as will be discussed below.

### 4.2. Activation of potassium by oxygen

The promoting effect of $O_2$ with respect to $NO_2$ (Figs. 10 and 11), suggests that oxygen activates the alkali phase. To fully consider this role of oxygen, it is important to discuss what state potassium is in following the pretreatment. It has been difficult to accurately assess the exact nature of the alkali sites on this multi component system. Details of the possible candidates are discussed elsewhere [11–15], with the leading candidates being $K_2O$ and one involving an exchange with alumina-based hydroxyl groups, Al–OK. For simplicity, we will assume $K_2O$ as it is also the most widely supported choice. The adsorption of

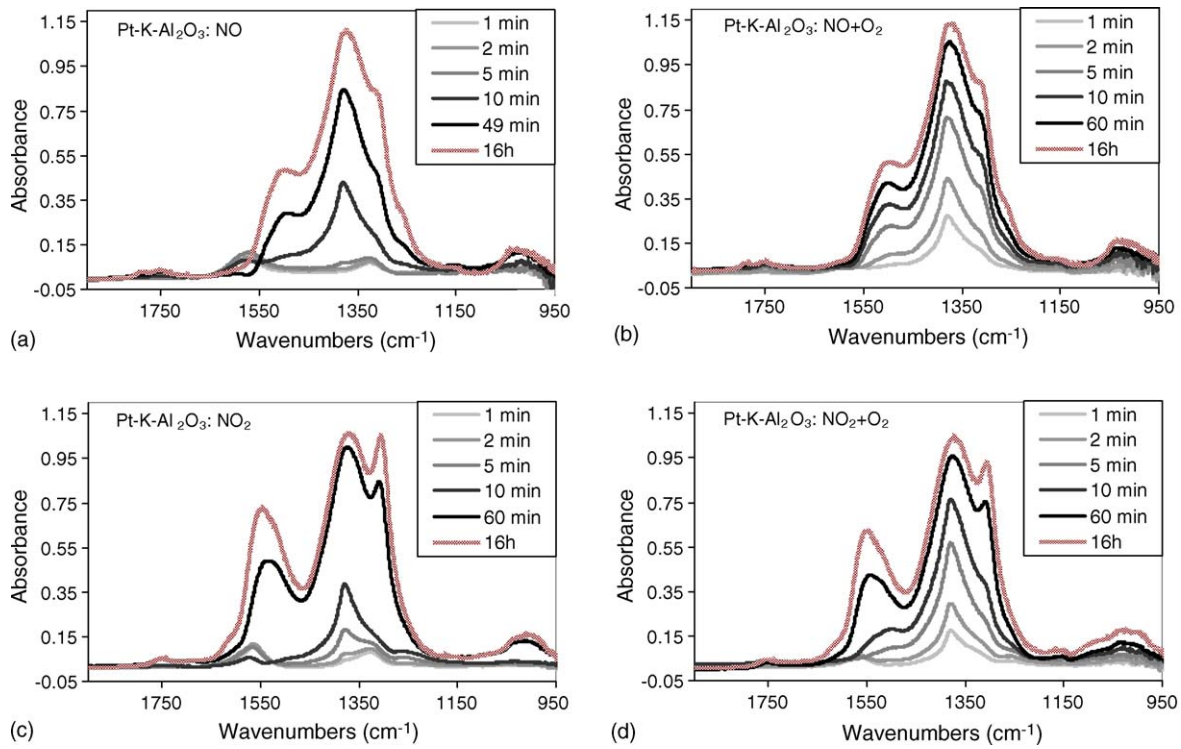


Fig. 9. DRIFT spectra of nitrate formation on $Pt/K/Al_2O_3$ at 250 °C with either: (a) 300 ppm NO, (b) 300 ppm NO and 12% $O_2$, (c) 300 ppm $NO_2$, or (d) 300 ppm $NO_2$ and 12% $O_2$. Experimental conditions: 50 sccm and $N_2$ balance; spectra recorded after times referenced on graphs with spectra at $t = 0$ subtracted.

a single oxygen atom onto $K_2O$ would lead to potassium peroxide, $K_2O_2$. Several groups have reported on the preferred stability of $K_2O_2$, $KO_2$, and even $K_2O_3$ in the presence of excess oxygen compared to $K_2O$ [43–46]; however, in the presence of $NO_x$ the deep oxidation, i.e. beyond $K_2O_2$, seems unlikely. A peroxide intermediate has also been proposed as an intermediate for barium-based LNTs, so this proposed route is in line with previously described LNT mechanisms [17,24,27].

As noted above, the most significant source of surface oxygen is associated with Pt sites, so it follows that potassium sites adjacent to Pt would be preferential activated by these oxygen atoms. The mechanism describing this approach follows from the NO oxidation discussion:

$$O_{2(g)} + Pt \rightarrow Pt{-}O_2 \quad (3')$$

$$Pt{-}O_2 + Pt \rightarrow 2Pt{-}O \quad (4')$$

$$2[Pt\text{-}O + K_2O \rightleftharpoons K_2O_2 + Pt] \quad (6)$$

Under conditions where $NO_2$ is in the gas-phase, i.e. when Eq. (5) shifts to the right, additional routes of adsorption must also be considered. The strength of the bond between Pt and O suggests that when $NO_2$ adsorbs on Pt it quickly dissociates to Pt–NO and Pt–O [42]:

$$NO_{2(g)} + 2\ Pt \rightleftharpoons Pt\text{-}NO + Pt\text{-}O \quad (7)$$

which is simply the reverse reaction from Eq. (5). Pt–O from this reaction would similarly react with adjacent $K^2O$ to form $K^2O^2$.

Fig. 11 also shows that the activation is not limited to sites near Pt, since $NO_2$ is stored at a significantly faster rate on $K/Al_2O_3$ when $O_2$ is present. The most plausible role of $O_2$ again involves the formation of potassium peroxide. Previous reports have shown this peroxide formation in the absence of a precious metal [43–45], so it follows that the peroxide formation can occur away from Pt through dissociative adsorption as follows:

$$O_{2(g)} + 2\ K_2O \rightleftharpoons 2\ K_2O_2 \quad (8)$$

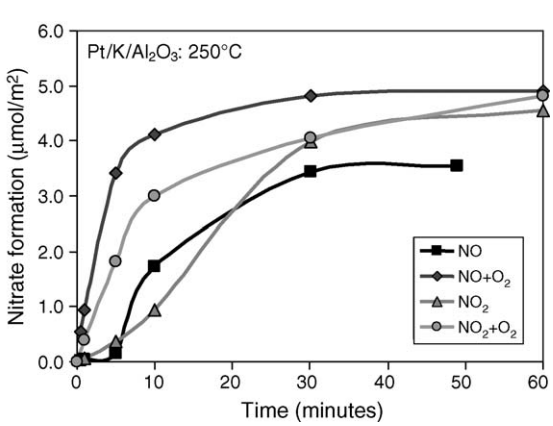


Fig. 10. Nitrate formation at 250 °C on the K-phase of $Pt/K/Al_2O_3$ under the listed $NO_x$ condition with respect to time.

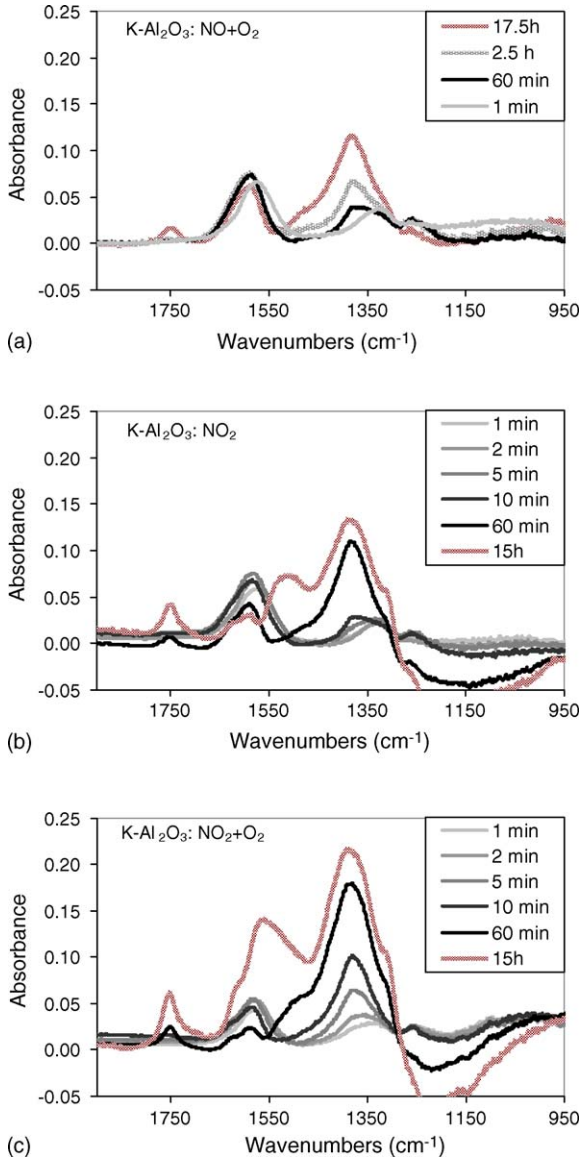


Fig. 11. DRIFT spectra of nitrate formation on $K/Al_2O_3$ at 250 °C with either: (a) 300 ppm NO and 12% $O_2$, (b) 300 ppm $NO_2$, or (c) 300 ppm $NO_2$ and 12% $O_2$. No significant nitrate formation observed for 300 ppm NO in the absence of $O_2$. Experimental conditions: 50 sccm and $N_2$ balance; spectra recorded after times referenced on graphs with spectra at $t = 0$ subtracted.

Since $NO_2$ is a stronger oxidizer than $O_2$, it will also contribute to $K_2O_2$ formation through the following route:

$$NO_{2(g)} + K_2O \rightleftharpoons K_2O_2 + NO_{(g)} \quad (9)$$

The resulting release of NO in this reaction would only have a significant role if Pt sites were available to oxidize it back to NO[2].

### 4.3. Nitrite formation

As shown in Fig. 6, nitrites only have a significant surface presence below 200 °C; however, understanding the route to their formation is important since they are probable intermediates at the higher temperatures even though they are not observed with DRIFTS. We will first discuss their formation at sites near Pt. With the prevalence of oxygen atoms and chemisorbed NO on the surface of Pt, the chemistry of nitrite formation is straightforward once $K_2O_2$ has been formed:

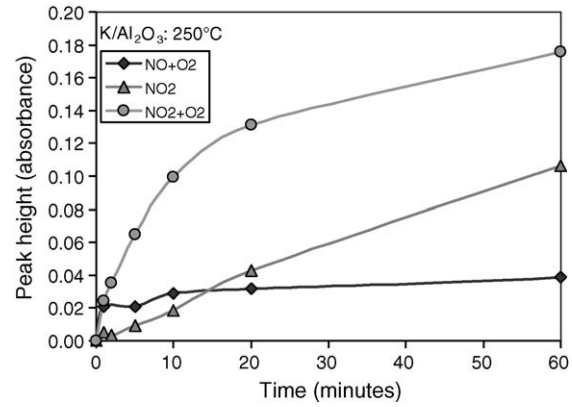


Fig. 12. Spectral height of 1375 $cm^{-1}$ for the adsorption of the given $NO_x$ condition at 250 °C on $K/Al_2O_3$.

$$Pt\text{-}NO + K_2O_2 \rightleftharpoons K\text{-}NO_2 + K\text{-}O + Pt \quad (10)$$

$$Pt\text{-}NO + K\text{-}O \rightleftharpoons K\text{-}NO_2 + Pt \quad (11)$$

On potassium sites away from Pt, $NO_2$ is clearly instrumental, and from Fig. 13, nitrites are present, so there must also be a route that does not involve Pt. It is difficult to identify the exact route, but it is possible to speculate the route invoking the guidelines from above, i.e. $K_2O$ can be oxidized to $K_2O_2$, and $NO_2$ is required for effective adsorption. The most likely route

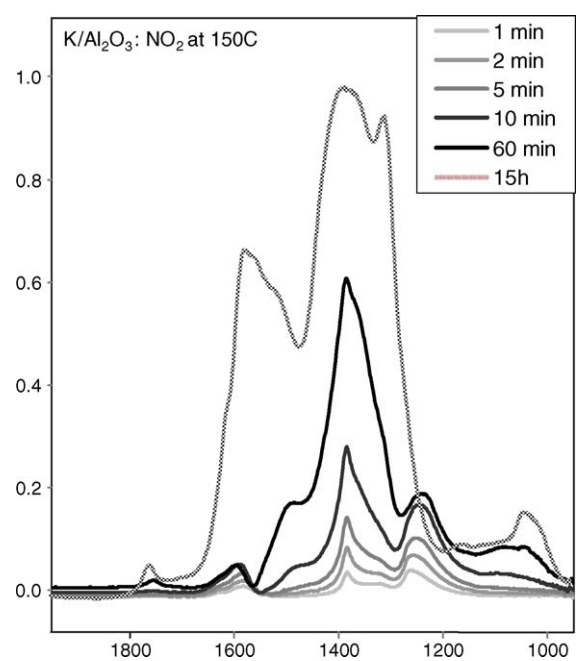


Fig. 13. DRIFT spectra of 300 ppm $NO_2$ flowing at 50 sccm over $K/Al_2O_3$ at 150 °C.

does not necessarily require activation of potassium, as $NO_2$ could directly adsorb leaving a K–O group:

$$NO_{2(g)} + K_2O \rightleftharpoons K\text{-}NO_2 + K\text{-}O \quad (12)$$

K–O would then either combine with another K–O group to make $K_2O_2$:

$$2K\text{-}O \rightleftharpoons K_2O_2 \quad (13)$$

or would be an active site for additional NO2 adsorption to directly form a nitrate:

$$NO_{2(g)} + K\text{-}O \rightleftharpoons K\text{-}NO_3 \quad (14)$$

It is also reasonable to suggest that NO could adsorb on the K–O intermediate to form a nitrite, but the results from Fig. 11(a) suggest that this is a kinetically negligible route away from Pt.

### 4.4. Nitrate formation

Eventually the nitrites discussed above will become nitrates, or will desorb. This is illustrated in an additional series of experiments that was performed to determine which process dominates at different temperatures. $Pt/K/Al_2O_3$ was loaded into the DRIFTS cell and pretreated at 450 °C, and then cooled to150 °C where 50 sccm of 300 ppm NO + 12% $O_2$ was adsorbed for 5 min. The reactor was then purged in Ar at 50 sccm. Fig. 14(a) shows the DRIFT spectra after adsorbing NO and $O_2$ for 5 min during the 10 min purge sequence. The nitrite at 1250 $cm^{-1}$ is clearly decreasing while the nitrate, 1380 $cm^{-1}$, continues to increase, illustrating that the nitrites are transitioning into nitrates. Fig. 14(b) is a plot of the peak heights during the purge sequence, which further illustrates the transition from nitrites to nitrates and also shows the $NO_x$ concentration as measured by mass spectrometry.[2] When the $NO_x$ concentration reaches zero at $t = 12$ min, the nitrite peaks are still diminishing, while the nitrates are still increasing. The sample was then heated to 300 °C while monitoring the DRIFT spectra. Upon heating either the nitrite will desorb, resulting only in an intensity decrease of the feature at 1250 $cm^{-1}$, or the nitrites will be oxidized to nitrates from surface oxygen, resulting in a synchronized nitrite decrease and nitrate increase. Fig. 15(a) shows the nitrite features, 1250 $cm^{-1}$, diminishing during the increase in temperature and the nitrates, 1380 $cm^{-1}$, increasing. The peak intensities are plotted in Fig. 15(b) and they show a correlation between the loss in intensity of nitrites with an increase in the nitrates; however, the mass spectrometer data in Fig. 15(b) also shows desorption of $NO_x$ shortly after beginning the ramp sequence. These results suggest that the nitrites are both being converted to nitrates up to at least 250 °C and being desorbed throughout the ramp.

The results presented throughout this paper demonstrate that nitrites are intermediates that are either further oxidized to nitrates or desorbed. The observation that the nitrite portion of

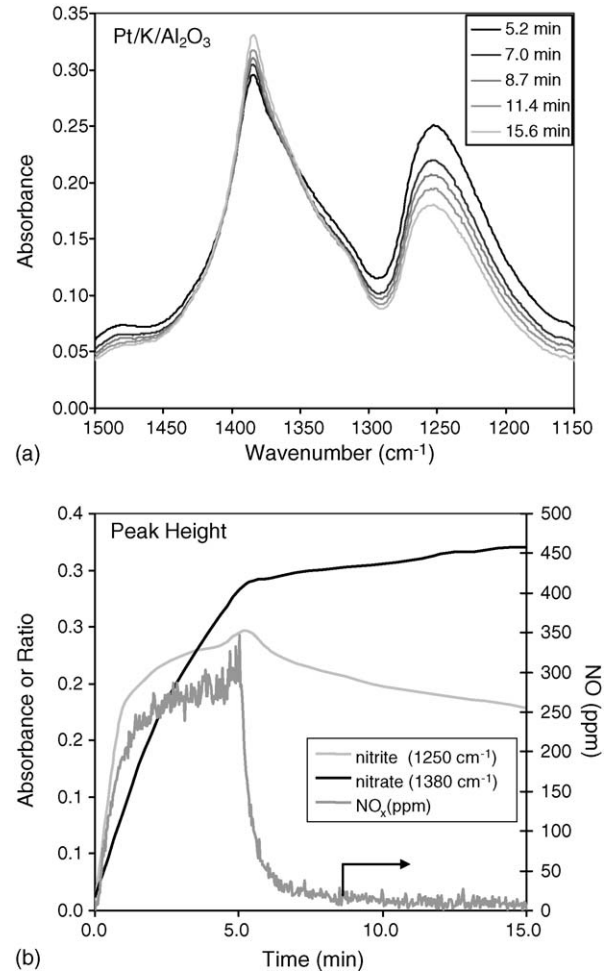


Fig. 14. (a) DRIFT spectra of nitrites (1250 $cm^{-1}$) and nitrates (1380 $cm^{-1}$) adsorbed from 300 ppm NO + 12% $O_2$ at 150 °C for 5 min, and then purged in Ar. At $t = 0$, NO + $O_2$ was introduced to the rector. All spectra are referenced to the initial fully reduced spectra at 150 °C. (b) Peak heights during the adsorption and purge steps are plotted on the left axis and $NO_x$ concentration is plotted on the right axis.

the spectra decreases when NO to $NO_2$ oxidation is favored over Pt, i.e. above 200 °C, suggests that the increased mobility of oxygen that enables the formation and desorption of $NO_2$ also contributes to the oxidation of nitrites to nitrates. It follows that near Pt the nitrate formation can be fully described by the following reactions described above:

$$4[NO_{(g)} + Pt \rightleftharpoons Pt\text{-}NO] \quad (2')$$

$$3[O_{2(g)} + Pt \rightarrow Pt\text{-}O_2] \quad (3')$$

$$3[Pt{-}O_2 + Pt \rightarrow 2Pt{-}O] \quad (4')$$

$$2[Pt\text{-}O + K_2O \rightleftharpoons K_2O_2 + Pt] \quad (6')$$

$$2[Pt\text{-}NO + K_2O_2 \rightleftharpoons K\text{-}NO_2 + K\text{-}O + Pt] \quad (10')$$

$$2[Pt\text{-}NO + K\text{-}O \rightleftharpoons K\text{-}NO_2 + Pt] \quad (11')$$

[2] The instrument is a residual gas analyzer quadropole mass spectrometer that can not distinguish between NO and $NO_2$, and therefore is calibrated for $NO_x$.

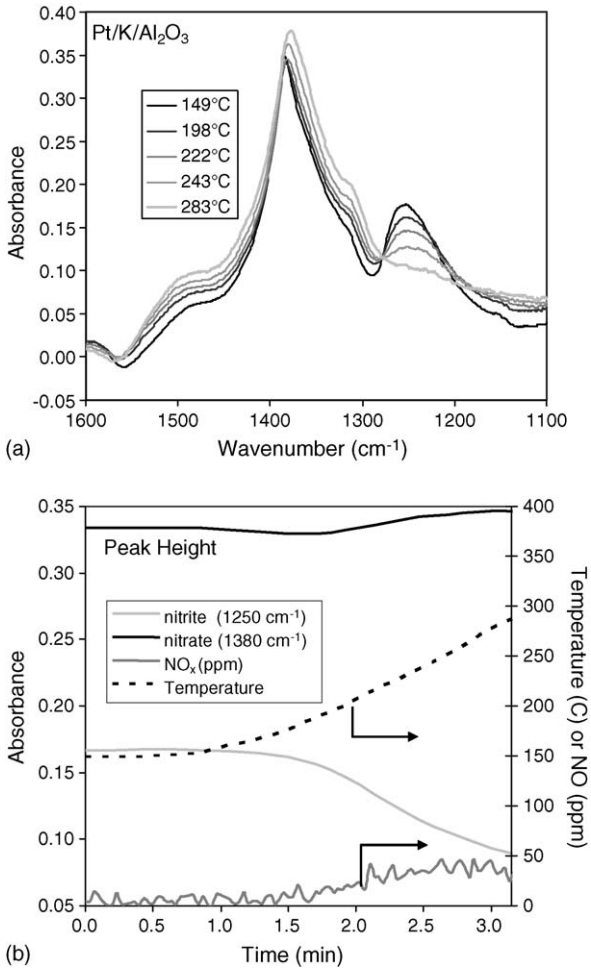


Fig. 15. (a) DRIFT spectra of nitrites (1250 $cm^{-1}$) and nitrates (1380 $cm^{-1}$) during the temperature ramp from 150 to 300 °C. The spectra were recorded after adsorbing 300 ppm NO + 12% $O_2$ at 150 °C for 5 min, and then purging in Ar. All spectra are referenced to the initial fully reduced spectra at 150 °C. (b) Peak height changes associated with heating $Pt/K/Al_2O_3$ with adsorbed nitrites and nitrates from 150 to 300 °C; heights are plotted on the left axis and $NO_x$ concentration is plotted on the right axis. At $t = 0$, the temperature was increased on the controller.

One additional reaction closes the catalytic sequence and results in the formation of the nitrate:

$$4[\text{Pt-O} + \text{K-NO}_2 \rightleftharpoons \text{Pt} + \text{K-NO}_3] \tag{15}$$

This sequence can be summarized in the following overall reaction that describes nitrate formation from NO adjacent to Pt:

$$4\text{NO}_{(g)} + 3\text{O}_2 + 2\text{K}_2\text{O} \xrightarrow{\text{Pt}} 4\text{KNO}_3 \tag{16}$$

This route does not directly invoke the formation of $NO_2$, but relies on the conditions that are necessary for $NO_2$ formation, i.e. oxygen atoms that are mobile or not strongly bound to Pt. It also details an adsorption route that requires the formation of a nitrite before forming the nitrate. There are no current results that suggest this route is not applicable at all temperatures, but the data does suggest that above 200 °C the nitrite intermediate is either quickly converted to a nitrate or desorbed.

Away from Pt, nitrites were also observed to be the precursor to nitrate formation, and since nitrites and nitrates were observed to be adsorbing simultaneously in Fig. 13, the proposed route invokes this observation. The initial adsorption is as proposed in the previous sub-section, where gaseous $NO_2$ adsorbs directly as a nitrite:

$$\text{NO}_{2(g)} + \text{K}_2\text{O} \rightleftharpoons \text{K-NO}_2 + \text{K-O} \tag{12'}$$

As mentioned earlier, the K–O group either combines with another K–O group to make $K_2O_2$, which subsequently oxidizes K–$NO_2$ via the following steps:

$$2\text{K-O} \rightleftharpoons \text{K}_2\text{O}_2 \tag{13'}$$

$$\text{K-NO}_2 + \text{K}_2\text{O}_2 \rightleftharpoons \text{K-NO}_3 + \text{K}_2\text{O} \tag{17}$$

or K–O adsorbs gas-phase $NO_2$ directly to form a nitrate:

$$\text{NO}_{2(g)} + \text{K-O} \rightleftharpoons \text{K-NO}_3 \tag{14'}$$

The overall reaction for either one of these routes is:

$$2\text{NO}_{2(g)} + \text{K}_2\text{O} \rightleftharpoons \text{K-NO}_3 + \text{K-NO}_2 \tag{18}$$

This sequence has satisfactory agreement with the spectra for $NO_2$ on $K/Al_2O_3$ at 150 °C during the first 10 couple of minutes, but at higher temperatures or during extended exposures the nitrite must still be oxidized to from the nitrate. In the absence of oxygen the nitrate can either be directly oxidized by $NO_2$:

$$\text{NO}_{2(g)} + \text{K-NO}_2 \rightleftharpoons \text{K-NO}_3 + \text{NO}_{(g)} \tag{19}$$

or $NO_2$ can form a peroxide intermediate that will oxidize the nitrite as follows:

$$\text{NO}_{2(g)} + \text{K}_2\text{O} \rightleftharpoons \text{K}_2\text{O}_2 + \text{NO}_{(g)} \tag{9'}$$

$$\text{K-NO}_2 + \text{K}_2\text{O}_2 \rightleftharpoons \text{K-NO}_3 + \text{K}_2\text{O} \tag{20}$$

Whichever path is followed, the release of NO is required to complete the sequence, and the overall expression becomes:

$$3\text{NO}_{2(g)} + \text{K}_2\text{O} \rightarrow 2\text{KNO}_3 + \text{NO}_{(g)} \tag{21}$$

This sequence represents the disproportionation of $NO_2$ on the potassium phase regardless of its proximity to Pt.

There is one final route to discuss that involves the direct nitrate formation from $NO_2$, without a nitrite intermediate. This route invokes many of the reactions discussed above, and assumes the $NO_2$ formation route described in reactions (2)–(5), but rather than the dissociative adsorption of $NO_2$ proposed in reaction (7), assumes non-dissociative adsorption. The mechanism proceeds as follows:

$$4[\text{NO}_{2(g)} + \text{Pt} \rightleftharpoons \text{Pt-NO}_2] \tag{22}$$

$$[\text{O}_{2(g)} + \text{Pt} \rightarrow \text{Pt}-\text{O}_2] \tag{3'}$$

$$[\text{Pt}-\text{O}_2 + \text{Pt} \rightarrow 2\text{Pt}-\text{O}] \tag{4'}$$

$$2[\text{Pt-O} + \text{K}_2\text{O} \rightleftharpoons \text{K}_2\text{O}_2 + \text{Pt}] \quad (6')$$

$$2[\text{Pt-NO}_2 + \text{K}_2\text{O}_2 \rightleftharpoons \text{K-NO}_3 + \text{K-O} + \text{Pt}] \quad (23)$$

$$4\text{NO}_{2(g)} + \text{O}_2 + 2\,\text{K}_2\text{O} \xrightarrow{\text{Pt}} 4\text{KNO}_3 \quad (24)$$

The overall reaction is then:

$$4\text{NO}_{2(g)} + \text{O}_2 + 2\text{K}_2\text{O} \xrightarrow{\text{Pt}} 4\text{KNO}_3 \quad (25)$$

Essentially, this route could occur anywhere an activated potassium group has formed, but due to the high sticking coefficient of $NO_2$ on Pt [47,48], it is assumed that the most kinetically significant route is through Pt sites. Furthermore, the disproportionation reaction above involves elements of this mechanism, so it could be argued that the direct nitrate formation on sites away from Pt is described in reaction (14).

## 5. Summary

DRIFTS has been used to elucidate key steps in the adsorption of $NO_x$ on $Pt/K/Al_2O_3$. The primary storage phase is an ionic nitrate that transitions through an ionic nitrite. Below 200 °C, the nitrite has a significant surface presence as storage is limited by oxygen mobility both on the K-phase and on Pt, but above 200 °C it is quickly oxidized to the nitrate on sites near Pt and non-adjacent sites, or it desorbs before being converted. Above 250 °C the stability of the adsorbates limit storage. The catalyst reaches saturation quickly, but the total amount of $NO_x$ stored is diminished. The findings in this study have suggested three central routes for the storage of $NO_x$ on $Pt/K/Al_2O_3$. The first two routes involve the adsorption of NO and $NO_2$ on a potassium storage site adjacent to Pt, and result in similar reaction pathways with the initial form of $NO_x$ altering the stoichiometry:

$$4\text{NO}_{(g)} + 3\text{O}_2 + 2\text{K}_2\text{O} \xrightarrow{\text{Pt}} 4\text{KNO}_3 \quad (16')$$

$$4\text{NO}_{2(g)} + \text{O}_2 + 2\text{K}_2\text{O} \xrightarrow{\text{Pt}} 4\text{KNO}_3 \quad (25')$$

A third route that occurs away from Pt involves a form of $NO_2$ disproportionation with the overall reaction:

$$3\text{NO}_{2(g)} + \text{K}_2\text{O} \rightarrow 2\text{KNO}_3 + \text{NO}_{(g)} \quad (21')$$

The support of these proposed mechanisms would be bolstered with kinetic modeling, and current efforts at ORNL are successfully employing these reactions to describe kinetics observed in bench flow reactors [49].

## Acknowledgements

The authors thank Dr. Louis Powell of the Oak Ridge Y-12 National Security Complex for use of the FT-IR spectrometer and DRIFTS accessory. This research was sponsored by the US Department of Energy under contract number DE-AC05-00OR22725 with the Oak Ridge National Laboratory, managed by UT-Battelle, LLC.

## References

[1] US Environmental Protection Agency (EPA), EPA420-F-00-057, Washington, DC, December 2000; US Government Printing Office, Federal Register, vol. 66, No. 12, January 18, 2001, p. 5135.
[2] N. Miyoshi, S. Matsumoto, K. Katoh, T. Tanaka, J. Harada, SAE Technical Paper 950809, 1995.
[3] N. Takahashi, H. Shinjoh, T. Iijima, T. Suzuki, K. Yamazaki, K. Yokota, H. Suzuki, N. Miyoshi, S.-I. Matsumoto, T. Tanizawa, T. Tanaka, S.-S. Tateishi, K. Kasahara, Catal. Today 27 (1996) 63.
[4] H. Shinjoh, N. Takahashi, K. Yokota, M. Sugiura, Appl. Catal. B 15 (1998) 189.
[5] M. Konsolakis, I.V. Yentekakis, Appl. Catal. B 29 (2001) 103.
[6] L.G. Neal, J.L. Haslbeck, H. Tseng, US Patent 475,599 (1988).
[7] K. Iwachido, H. Tanada, T. Watanabe, N. Yamada, O. Nakayama, H. Ando, M. Hori, S. Taniguchi, N. Noda and F. Abe, SAE Technical Paper 2001-01-1298.
[8] D. Dou, J. Balland, SAE Technical Paper 2002-01-0734.
[9] L.J. Gill, P.G. Blakeman, M.V. Twigg, A.P. Walker, Top. Catal. 28 (2004) 157.
[10] W.S. Epling, L.E. Campbell, A. Yezerets, N.W. Currier, J.E. Parks, Catal. Rev. 46 (2004) 163.
[11] W.H.J. Stork, G.T. Pott, J. Phys. Chem. 78 (1974) 2496.
[12] B.W. Krupay, Y. Amenomiya, J. Catal. 67 (1981) 362.
[13] B.W. Krupay, Y. Amenomiya, J. Catal. 76 (1982) 345.
[14] M. Kantschewa, E.V. Albano, G. Ertl, H. Knözinger, Appl. Catal. 8 (1983) 71.
[15] T.J. Toops, D.B. Smith, W.P. Partridge, Appl. Catal. B 58 (2005) 245.
[16] T.J. Toops, D.B. Smith, J.E. Parks, W.S. Epling, W.P. Partridge, Appl. Catal. B 58 (2005) 255.
[17] T. Lesage, C. Verrrier, P. Bazin, J. Saussey, S. Malo, C. Hedouin, G. Blanchard, M. Daturi, Top. Catal. 30/31 (2004) 31.
[18] E. Fridell, H. Persson, B. Westerberg, L. Olsson, M. Skoglundh, Catal. Lett. 66 (2000) 71.
[19] E. Fridell, M. Skoglundh, B. Westerberg, S. Johansson, G. Smedler, J. Catal. 183 (1999) 196.
[20] Y. Li, S. Roth, J. Dettling, T. Beutel, Top. Catal. 16/17 (2001) 139.
[21] X. Li, M. Meng, P. Lin, Y. Fu, T. Hu, Y. Xie, J. Zhang, Top. Catal. 22 (2003) 111.
[22] H. Mazoul, J.F. Brilhac, P. Gilot, Appl. Catal. 20 (1999) 47.
[23] F. Prinetto, G. Ghiotti, I. Nova, L. Lietti, E. Tronconi, P. Forzatti, J. Phys. Chem. B 105 (2001) 12732.
[24] L. Olsson, E. Fridell, M. Skoglundh, B. Andersson, Catal. Today 73 (2002) 263.
[25] L. Lietti, P. Forzatti, I. Nova, E. Tronconi, J. Catal. 204 (2001) 175.
[26] F. Rodrigues, L. Juste, C. Potvin, J.F. Tempere, G. Blanchard, G. Djega-Mariadassou, Catal. Lett. 72 (2002) 59.
[27] N.W. Cant, M.J. Patterson, Catal. Today 73 (2002) 271.
[28] P.J. Schmitz, R.J. Baird, J. Phys. Chem. B 106 (2002) 4172.
[29] I. Nova, L. Catoldi, L. Lietti, E. Tronconi, P. Forzatti, F. Prinetto, G. Ghiotti, J. Catal. 222 (2004) 377.
[30] G.L. Powell, M. Milosevic, J. Lucania, N.J. Harrick, Appl. Spectrosc. 46 (1992) 111.
[31] A.A. Davydov, in: C.H. Rochester (Ed.), Infrared Spectroscopy of Adsorbed Species on the Surface of Transition Metal Oxides, John Wiley & Sons, Chichester, England, 1990.
[32] B. Klingenberg, M.A. Vannice, Appl. Catal. B 21 (1999) 19.
[33] B. Westerberg, E. Fridell, J. Mol. Catal. A 165 (2001) 249.
[34] A. Bourane, O. Dulaurent, S. Salasc, C. Sarda, C. Bouly, D. Bianchi, J. Catal. 204 (2001) 77.
[35] S.-J. Huang, A.B. Walters, M.A. Vannice, Appl. Catal. B 26 (2000) 101.
[36] B. Klingenberg, M.A. Vannice, Chem. Mater. 8 (1996) 2755.
[37] W.S. Kijlstra, D.S. Brands, E.K. Poels, A. Bliek, J. Catal. 171 (1997) 208.
[38] J. Segner, C.T. Campbell, G. Doyen, G. Ertl, Surf. Sci. 138 (1984) 505.
[39] Z.M. Liu, Y. Zhou, F. Solymosi, J.M. White, Surf. Sci. 245 (1991) 289.

[40] J.B. Bates, G.E. Boyd, Appl. Spectrosc. 27 (1973) 204.
[41] L. Olsson, H. Persson, E. Fridell, M. Skoglundh, B. Andersson, J. Phys. Chem. B 105 (2001) 6895.
[42] S.S. Mulla, N. Chen, W.N. Delgass, W.S. Epling, F.H. Ribeiro, Catal. Lett. 100 (2005) 267.
[43] B. Lamontagne, F. Semond, D. Roy, Surf. Sci. 327 (1995) 371.
[44] K. Nagase, M. Itoh, A. Watanabe, J. Therm. Anal. Calorim. 70 (2002) 329.
[45] D.V. Chakrov, P. Sjovall, B. Kasemo, J. Phys. Condens. Matter 5 (1993) 2903.
[46] G.H. Rocker, C. Huang, C.L. Cobb, J.D. Redding, H. Metiu, R.M. Martin, Surf. Sci. 250 (1991) 33.
[47] J. Segner, W. Vielhaber, G. Ertl, Isr. J. Chem. 22 (1982) 375.
[48] D.H. Parker, B. Koel, J. Vac. Sci. Technol. A 8 (1990) 2585.
[49] V.K. Chakravarthy, J.-S. Choi, T.M. Miller, C.S. Daw, Appl. Catal. B, in preparation.